International Journal of

Railway Research

Iran University of
Science and Technology

Chaotic Response and Bifurcation Analysis of a Timoshenko Beam with Backlash Support Subjected to Moving Masses

A. Ariaei[*,1], M. Kouchaki[1], S. Ziaei-Rad[2]

[1]Department of Mechanical Engineering, University of Isfahan, Iran

[2]Department of Mechanical Engineering, Isfahan University of Technology, Iran

A B S T R A C T

A simply supported Timoshenko beam with an intermediate backlash is considered. The beam equations of motion are obtained based on the Timoshenko beam theory by including the dynamic effect of a moving mass travelling along the vibrating path. The equations of motion are discretized by using the assumed modes technique and solved using the Runge–Kutta method. The analysis methods employed in this study are the dynamic trajectories of the beam midpoint, power spectra, Poincare´ maps, bifurcation diagrams and Lyapunov exponents. The dimensionless backlash gap coefficient and the moving mass speed are used as control parameters. The numerical results reveal that the system exhibits a diverse range of periodic, sub-harmonic, and chaotic behaviors. The onset of chaotic motion is identified from the phase diagrams, power spectra, Poincaré maps, and Lyapunov exponents of the system. Therefore, the main aim of this study is to provide a better understanding of the characteristics and dynamic behaviors of the beams subjected to moving masses.

Keywords: Non-ideal support, Chaotic vibration, Timoshenko beam, Moving mass, Bifurcation diagram.

1. Introduction

The effect of moving loads and masses on structures and machines is an important problem both in the field of transportation and in the design of machining processes. A moving mass (or moving load) produces larger deflections and higher stresses than does an equivalent load applied statically. These deflections and stresses are functions of both time and speed of the moving loads.

For more than a century, the analysis of continuous elastic systems subjected to moving masses has been the subject of interest in many diverse fields such as civil and aerospace engineering [1]. Historically, the problem first arose in the design of railway bridges, and later in other transportation engineering problems such as the design of bridges, guideways, overhead

cranes, cableways, rails, roadways, runways, tunnels and pipelines with moving masses [2].

Recent investigations include the work of Chen [3], who showed how a general finite element code may be used to efficiently model bridge superstructures (such as I-shaped girders) under the variable moving load. Wu and Thompson [4] studied the non-linear properties of railroad track foundations under a single moving wheel load. Todd and Vohra [5] presented a theoretical approach to reconstruct the beam shape under static or moving load from strain measurements at a number of locations along beam length and taking shear deformation into account. The method was successfully applied to a two-span beam under a static load, and a simply supported beam under a moving load. A more recent book by Fryba [6] includes analyses of moving masses on a beam under different loading conditions.

[*] Corresponding Author
Email Address: ariaei@eng.ui.ac.ir

Akin and Mofid [7-8] developed the so-called discrete element technique (DET) for the vibration analysis of Euler-Bernoulli beams subjected to a concentrated moving mass. Younesian et al. [9] presented a generalized technique for the moving load problem. They studied the vibration response of a Timoshenko beam supported by a viscoelastic foundation with randomly distributed parameters along the beam length and subjected to a harmonic moving load. The method they presented was based on measurements gathered by a moving vehicle, which is of significant engineering importance. Yavari et al. [10] extended the work of Mofid to a case with lumped masses and Timoshenko beams, i.e. they were able to consider the effect of shear deformation and rotary inertia and Ziaei et al. [11] studied a Timoshenko beam under uniform partially distributed moving masses.

In the last decade, chaos has become a focal point for non-linear problems in subjects ranging from physics and chemistry to biology and economics [12–16]. Most mechanical systems are non-linear in nature, and can be described by the non-linear equations of motion. It has been realized that the responses of many non-linear dynamical systems do not follow simple, regular or predictable trajectories. A large number of studies have shown that chaotic phenomena may occur in many non-linear dynamical systems [17–23].

In vibrations of continuous systems, types of support conditions are important and have direct effect on the solutions and natural frequencies. In real system applications, usually the support type that best resembles the behavior is selected. However, the real system behavior may deviate from the idealized support conditions. For example, if the beam is simply supported, the ideal conditions require deflections and moments to be zero at the supports. In reality, however, small deviations from the ideal conditions indeed occur. On the other hand, the hole and pin assembly may have small gaps and/or friction which may introduce small deflections and/or moments at its ends. To represent such behaviour, a non-ideal boundary condition concept has been recently proposed [24–26]. Pakdemirli and Boyaci [24] studied linear beam problems of different support conditions and an axially moving string problem. They also investigated a non-linear beam problem with stretching [25]. Finally, they considered the forced damped case with a non-ideal simple support at an intermediate point and contracted ideal and non-ideal frequencies [26]. Lin and Ewins [27] presented detailed numerical and experimental studies on the chaotic dynamic behavior on nonlinear

mechanical systems with backlash. Such systems arise in engineering structures in which components make intermittent contact due to the existence of clearance.

The main purpose of this article is to analyze the chaotic response of a Timoshenko beam subjected to moving masses with a non-ideal support in between. The support is modeled as a backlash. It is considered that a new mass enters the beam domain from the left as soon as the old one exits it from the right, the process then being repeated for an arbitrary number. First, an analytical formulation is presented for simply supported beam subjected to moving masses. The equations of motion are discretized by using the assumed modes technique and solved using the fourth Runge–Kutta method. Next, by considering the non-ideal support of the midpoint of the beam, the critical values for the control parameters, i.e. the dimensionless gap coefficient and the moving mass speed, are detected by the bifurcation diagram. Finally, the behavior of the system (in some critical values of the control parameter) is presented by time history, phase plane, Poincare maps, power spectrum and Lyapunov Exponents.

2. Problem formulation
1. Governing equations of a Timoshenko beam under a moving mass

A simply supported Timoshenko beam of length L with a backlash support in between is considered as in Figure 1.
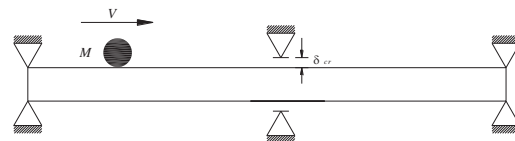

Figure 1: A beam with non-ideal support in between subjected to moving masses

For modeling of this problem, the stiffness of the support is represented by a linear spring (Figure 2). By using Timoshenko beam theory, the equation of motion for each segment, assumed to have uniform cross section, is [28].

$$\rho A \frac{\partial^2 Y}{\partial T^2} - \kappa AG \left(\frac{\partial^2 Y}{\partial X^2} - \frac{\partial \Phi}{\partial X} \right) = P(T)\delta(X - VT) + f(T)\delta\left(X - L_s\right) \tag{1a}$$

$$EI \frac{\partial^2 \Phi_{(i)}}{\partial X^2} + \kappa AG \left(\frac{\partial Y_{(i)}}{\partial X} - \Phi_{(i)} \right) - \rho I \frac{\partial^2 \Phi_{(i)}}{\partial T^2} = 0 \tag{1b}$$

where Y and Φ are deflection and rotation of the beam, respectively. Also, ρ is the beam's volumetric density, I is the cross-sectional moment of inertia, A is the cross sectional area, E is Young's modulus of elasticity, G is the shear modulus, and κ is the shear correction factor in Timoshenko beam theory which is a function of the cross-section and the Poisson ratio υ [29]. The terms $\delta(X - \xi(T))$ and $\delta(X - L_s)$ denote the Dirac delta function which ζ and L_s define the moving mass and backlash support locations, respectively.
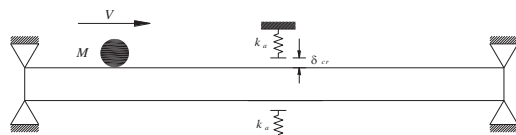
Figure 2: Non-ideal support in between
is replaced by a linear spring

The expression for $P(T)$ depends on the analytical model used to represent the moving load. In the case of the moving mass, it is modeled by the following relation

$$P(T) = M\{g - \Lambda[Y_i(X,T)]_{X=\xi(T)}\} \qquad (2)$$

where M is the moving mass, g is the acceleration due to gravity, and $\Lambda[\bullet]$ is a linear differential operator that takes into account the acceleration of the moving mass [30]

$$\Lambda[\bullet] = \left(\frac{\partial^2}{\partial T^2} + 2\dot{\xi}\frac{\partial^2}{\partial X \partial T} + \dot{\xi}^2\frac{\partial^2}{\partial X^2} + \ddot{\xi}\frac{\partial}{\partial X}\right)[\bullet] \qquad (3)$$

In this expression $\dot{\xi}$ and $\ddot{\xi}$ are the speed and translational acceleration of the moving mass, respectively. Also, the term $\left(2\dot{\xi}^2\frac{\partial^2[Y_\xi]}{\partial X \partial T}\right)$ is derived from Coriolis force and plays the role of damping. However, the term $\left(\dot{\xi}^2\frac{\partial^2[Y_\xi]}{\partial X^2}\right)$, which is derived from centrifugal force (normal to the beam), plays the role of weakening the bending stiffness of the system. Also, the terms $\left(\frac{\partial^2[Y_\xi]}{\partial T^2}\right)$ and $\left(\ddot{\xi}\frac{\partial[Y_\xi]}{\partial X}\right)$ are from inertia force and the force derived from moving mass translational acceleration, respectively. Moreover, $f(T)$ is the force exerted by the non-ideal support where its magnitude is defined as

$$\begin{cases} f = k_a\left(\left|\delta_m\right| - \delta_{cr}\right) & \left|\delta_m\right| \geq \delta_{cr} \\ f = 0 & \left|\delta_m\right| < \delta_{cr} \end{cases} \qquad (4)$$

In the above equation, k_a is the stiffness of the linear spring, δ_m is the deflection of the beam in the non-ideal support location and δ_{cr} is the distant between the beam and the non-ideal support at rest.

From Eq. (2) it is apparent that the interaction force depends on the beam response itself. The boundary conditions of the simply supported beam are

$$Y(0,T) = \Phi'(0,T) = 0 \qquad (5a)$$

$$Y(L,T) = \Phi'(L,T) = 0 \qquad (5b)$$

By introducing the following quantities to the previous equations:

$$y = \frac{Y}{L}, \quad x = \frac{X}{L}, \quad t = \frac{T}{\sqrt{L}}, \quad v = \frac{V}{\sqrt{L}}, \quad \zeta = \frac{\xi(T)}{L}, \quad l_s = \frac{L_s}{L} \qquad (6)$$

Thus, for each segment, Eq. (1a, b) can then be expressed as

$$\rho A \frac{\partial^2 y}{\partial t^2} - \frac{\kappa AG}{L}\left(\frac{\partial^2 y}{\partial x^2} - \frac{\partial \phi}{\partial x}\right) = \frac{P(t)}{L}\delta(x - \zeta(t)) + \frac{f(t)}{L}\delta(x - l_s) \qquad (7a)$$

$$\frac{EI}{L^3}\frac{\partial^2 \phi}{\partial x^2} + \frac{\kappa AG}{L}\left(\frac{\partial y}{\partial x} - \phi\right) - \frac{\rho I}{L^2}\frac{\partial^2 \phi}{\partial t^2} = 0 \qquad (7b)$$

where

$$P(t) = M\left\{g - \Gamma[y(x,t)]\Big|_{x=\zeta(t)}\right\} \qquad (8a)$$

$$\Gamma[\bullet] = \left(\frac{\partial^2}{\partial t^2} + 2\dot{\zeta}\frac{\partial^2}{\partial x \partial t} + \dot{\zeta}^2\frac{\partial^2}{\partial x^2} + \ddot{\zeta}\frac{\partial}{\partial x}\right)[\bullet] \qquad (8b)$$

In the above equation, $\Gamma[\bullet]$ is the non-dimensional of $\Lambda[\bullet]$ and is equal to $L\,\Lambda[\bullet]$.

2. Eigenvalues and eigenfunctions of the simply supported Timoshenko beam

The eigensolutions of the beam are derived letting the forcing term, $P(t)\delta(x - \zeta(t))$ and $f(t)\delta(x - l_s)$, to be zero. The solutions for the other boundary conditions can also be obtained through similar procedures. Using some rearrangement and the separable solutions: $y(x,t) = w(x)e^{i\omega t}$ and $\phi(x,t) = \varphi(x)e^{i\omega t}$ in Eq. (7a, b) leads to an associated eigenvalue problem [28]:

$$w^{iv}(x) + (\sigma + \tau)w''(x) - (\alpha - \sigma\tau)w(x) = 0 \qquad (9a)$$

$$\varphi^{iv}(x) + (\sigma + \tau)\varphi''(x) - (\alpha - \sigma\tau)\varphi(x) = 0 \tag{9b}$$

where

$$\sigma = \frac{\rho L \omega^2}{E}, \quad \tau = \frac{\rho L \omega^2}{\kappa G}, \quad \alpha = \frac{A\rho L^3 \omega^2}{EI} \tag{10}$$

A closed-form solution to this eigenvalue problem can be obtained by employing the transfer matrix method [28, 31]. The general solutions of Eqs. (9a, b), for each segment, are [28]

$$w(x) = A\cosh\lambda_1(x - x_0) + B\sinh\lambda_1(x - x_0) + C\cos\lambda_2(x - x_0) + D\sin\lambda_2(x - x_0) \tag{11a}$$

$$\varphi(x) = Bq_1\cosh\lambda_1(x - x_0) + Aq_1\sinh\lambda_1(x - x_0) - Dq_2\cos\lambda_2(x - x_0) + Cq_2\sin\lambda_2(x - x_0) \tag{11b}$$

where

$$\lambda_1 = \left[\sqrt{\left(\frac{\sigma - \tau}{2}\right)^2 + \alpha} - \frac{\sigma + \tau}{2}\right]^{1/2}, \quad \lambda_2 = \left[\sqrt{\left(\frac{\sigma - \tau}{2}\right)^2 + \alpha} + \frac{\sigma + \tau}{2}\right]^{1/2}, \tag{12}$$

$$\lambda_3 = \sqrt{\tau}, \quad q_1 = \frac{(\lambda_3^2 + \lambda_1^2)}{\lambda_1}, \quad q_2 = \frac{(\lambda_3^2 - \lambda_2^2)}{\lambda_2}$$

For case of a simply supported beam, the corresponding boundary conditions of Eqs. (5a, b) can thus be expressed as

$$Y(0,T) = 0 \rightarrow w(0) = 0 \tag{13a}$$

$$\Phi'(0,T) = 0 \rightarrow \varphi'(0) = 0 \tag{13b}$$

Satisfying the above boundary conditions at the beam left support leads to

$$A = C = 0 \tag{14}$$

By satisfying the boundary conditions at the right support, one can be obtained that

$$\mathbf{S}_{2\times4}\begin{Bmatrix} A \\ B \\ C \\ D \end{Bmatrix} = \begin{Bmatrix} 0 \\ 0 \end{Bmatrix} \tag{15}$$

where

$$\mathbf{S}_{2\times4} = \begin{bmatrix} \cosh\lambda_1 & \sinh\lambda_1 & \cos\lambda_2 & \sin\lambda_2 \\ q_1\lambda_1\cosh\lambda_1 & q_1\lambda_1\sinh\lambda_1 & q_2\lambda_2\cos\lambda_2 l_{n+1} & q_2\lambda_2\sin\lambda_2 \end{bmatrix} \tag{16}$$

Substitution of Eq. (14) into Eq. (15) leads to

$$\mathbf{S}_{2\times4}\begin{Bmatrix} A \\ B \\ C \\ D \end{Bmatrix} = \mathbf{S}_{2\times4}\begin{Bmatrix} 0 \\ B \\ 0 \\ D \end{Bmatrix} = \begin{Bmatrix} 0 \\ 0 \end{Bmatrix} \tag{17}$$

Therefore, the existence of non-trivial solutions requires

$$\det\begin{vmatrix} \sinh\lambda_1 & \sin\lambda_2 \\ q_1\lambda_1\sinh\lambda_1 & q_2\lambda_2\sin\lambda_2 \end{vmatrix} = 0 \tag{18}$$

This determinant provides the single equation for the solution of eigenvalue ω. This is a matrix of only 2×2 dimensions, therefore, it is a simpler process to obtain the corresponding characteristic equation. The coefficients of the eigenfunctions, $w(x)$ and $\varphi(x)$ are obtained by back substitution into Eqs. (17) and (11).

3. Forced response

The original equation of motion, Eqs. (7a, b), is rewritten here:

$$\rho A \frac{\partial^2 y}{\partial t^2} - \frac{\kappa AG}{L}\left(\frac{\partial^2 y}{\partial x^2} - \frac{\partial\phi}{\partial x}\right) = \frac{P(t)}{L}\delta(x - \zeta(t)) + \frac{f(t)}{L}\delta(x - l_s) \tag{19a}$$

$$\frac{EI}{L^3}\frac{\partial^2\phi}{\partial x^2} + \frac{\kappa AG}{L}\left(\frac{\partial y}{\partial x} - \phi\right) - \frac{\rho I}{L^2}\frac{\partial^2\phi}{\partial t^2} = 0 \tag{19b}$$

Using the modal expansion theory, the forced response $y(x,t)$ and $\phi(x,t)$ of this system can be expressed as

$$y(x,t) = \sum_{k=1}^{N} w_k(x)p_k(t) \tag{20a}$$

$$\phi(x,t) = \sum_{k=1}^{N} \varphi_k(x)p_k(t) \tag{20b}$$

where $p_k(t)$ are the generalized coordinates (time functions) for the elastic deflection and orientation of the beam element. The functions $w_k(x)$ and $\varphi_k(x)$ are the respective transverse and rotational eigenfunctions (modal shapes) of a Timoshenko beam. The use of same time functions, $p_k(t)$, in the Galerkin approximation is a common practice and the standard assumption that has been utilized by many researchers in other areas of mechanics. In reference [32], two different time functions were used for $y(x,t)$ and $\phi(x,t)$, respectively. The results showed that the difference in obtained solutions is small and concluded that assuming the same time functions for both variables $y(x,t)$ and $\phi(x,t)$ is reasonable. Substituting Eqs. (20a, b) into Eqs. (19a, b), yields

$$\sum_{k=1}^{N} \left\{ \rho A w_k(x) \ddot{p}_k(t) - \kappa AG \left(w_k'' - \varphi_k' \right) p_k(t) \right\} = \frac{P(t)}{L} \delta(x - \zeta(t)) + \frac{f(t)}{L} \delta(x - l_s) \quad (21a)$$

$$\sum_{k=1}^{N} \left\{ \begin{array}{l} EI \varphi_k''(x) p_k(t) + \\ \kappa AG \left(w_k' - \varphi_k \right) p_k(t) - \rho I \varphi_k(x) \ddot{p}_k(t) \end{array} \right\} = 0 \quad (21b)$$

On the other hand, from the free vibration analysis we have

$$-\kappa AG \left(w_k'' - \varphi_k' \right) = \rho A \omega_k^2 w_k(x) \quad (22a)$$

$$EI \varphi_k''(x) + \kappa AG \left(w_k' - \varphi_k \right) = -\rho I \omega_k^2 \varphi_k(x) \quad (22b)$$

where ω_k is the kth natural frequency of the beam. Substituting Eqs. (22a, b) into Eqs. (21a, b) results in

$$\rho A \sum_{k=1}^{N} w_k(x) \left[\ddot{p}_k(t) + \omega_k^2 p_k(t) \right] = \frac{P(t)}{L} \delta(x - \zeta(t)) + \frac{f(t)}{L} \delta(x - l_s) \quad (23a)$$

$$\rho I \sum_{k=1}^{N} \varphi_k(x) \left[\ddot{p}_k(t) + \omega_k^2 p_k(t) \right] = 0 \quad (23b)$$

In order to solve for $p_k(t)$ from Eqs. (23a, b), the orthogonality conditions [32] of

$$\int_0^1 \left[w_i(x) w_j(x) + \frac{I}{AL^2} \varphi_i(x) \varphi_j(x) \right] dx = \delta_{ij} \quad (24)$$

are utilized, where $i, j = 1,2,..., N$ and δ_{ij} is the Kronecker delta. Multiplying Eq. (23a) by $w_k(x)$ and Eq. (23b) by $\varphi_k(x)$, adding each side together, integrating over the entire length of the beam, and with the use of the orthogonality relationship (24), we get

$$\ddot{p}_k(t) + \omega_k^2 p_k(t) = \frac{1}{\rho AL} \left[P(t) w_k(\zeta(t)) + f(t) w_k(l_s) \right] = Q_k(t) \quad (25)$$

Again, here $w_k(x)$ are eigenfunctions of the cracked beam system. Using Eqs. (20) and (8b) in Eq. (8a), the beam-moving mass interaction force is rewritten as

$$P(t) = M \left\{ g - \sum_{k=1}^{N} w_k \ddot{p}_k + 2\dot{\zeta} w_k' \dot{p}_k + \left[\dot{\zeta}^2 w_k'' + \ddot{\zeta} w_k' \right] p_k \right\} \quad (26)$$

where the prime denotes differentiation with respect to x.

The right-hand side of Eqs. (25) depends on the function $P(t)$ which, in turn, depends on the

coefficients $p_k(t)$ (Eq. (26)). It is clear, then, that Eqs. (25) are a set of coupled second order linear differential equations that can be solved by different techniques such as those mentioned in references [30] and [33].

After determining $p_k(t)$ from Eq. (25) and by using of known initial conditions, the forced response solutions $y(x,t)$ and $\phi(x,t)$ can then be reconstructed from Eqs. (20a, b). In order to simplify the program implementation, let us introduce the following functions [30]

$$\upsilon_{k,p}(x) = w_k^{(p)}(x) \qquad k = 1,2,..., N \quad (27)$$

Also, for extraction of the steady state response, the following equation is used instead of equation (25)

$$\ddot{p}_k(t) + 2 r_k \omega_k \dot{p}_k(t) + \omega_k^2 p_k(t) = Q_k(t) \quad (28)$$

where r_k is defined as the viscous damping of the kth mode. Using the Eq. (28) the transient response can be neglected and it is reasonable to assume that only the steady state response remains after a short period of time. Finally, by using the method described in [30] and by adding the effect of damping, a compact matrix form is obtained as

$$M(t) \ddot{p}(t) + D(t) \dot{p}(t) + K(t) p(t) = Mg V_0[\zeta(t)] \quad (29)$$

where p(t) is an n-dimensional vector collecting the unknowns $p_r(t)$, $V_p(x) = [\upsilon_{1,p}(x), \upsilon_{2,p}(x), ..., \upsilon_{N,p}(x)]^T$ and the system matrices are given by

$$M(t) = I_N + M V_0[\zeta(t)] V_0^T[\zeta(t)] \quad (30a)$$

$$D(t) = 2 r\Omega + 2M \dot{\zeta}(t) V_0[\zeta(t)] V_1^T[\zeta(t)] \quad (30b)$$

$$K(t) = \Omega^2 + M V_0[\zeta(t)] \left\{ \dot{\zeta}^2(t) V_2^T[\zeta(t)] + \ddot{\zeta}(t) V_1^T[\zeta(t)] \right\} \quad (30c)$$

in which I_N is an n-dimensional identity matrix and $2r\Omega$ and Ω^2 are equal to

$$2 r\Omega = \text{diag} \left[2 r_1 \omega_1, 2 r_2 \omega_2, ..., 2 r_N \omega_N \right]$$

$$\Omega^2 = \text{diag} \left[\omega_1^2, \omega_2^2, ..., \omega_N^2 \right] \quad (31)$$

Now, the following definition is considered

$$\Psi_0(x) = \left[\varphi_1(x), \varphi_2(x), ..., \varphi_N(x) \right]^T \quad (32)$$

The initial conditions associated with Eq. (29) are written as

$$p(0) = \int_0^1 \left[y_0(x)V_0(x) + \frac{I}{AL^2}\phi_0(x)\psi_0(x) \right]dx \qquad (33a)$$

$$\dot{p}(0) = \int_0^1 \left[\dot{y}_0(x)V_0(x) + \frac{I}{AL^2}\dot{\phi}_0(x)\psi_0(x) \right]dx \qquad (33b)$$

The set of Eq. (29) can be solved using a different number of numerical integration schemes. The solution procedure presented has been implemented in Matlab code. Once the vector p(t) has been obtained, one can calculate the beam response according to the expressions

$$y(x,t) = V_0^T(x)p(t) \qquad (34a)$$

$$\phi(x,t) = \Psi_0(x)p(t) \qquad (34b)$$

$$M(x,t) = EI\,\Psi_1^T(x)p(t) \qquad (34c)$$

$$Q(x,t) = \kappa AG\left[V_1^T(x) - \Psi_0^T(x)\right]p(t) \qquad (34d)$$

Finally, if the following terms are inserted into Eq. (29) for the mass, damping and stiffness matrices respectively, the governing equations for the special case of a moving force problem will be obtained.

$$M(t) = I_N \qquad (35a)$$

$$D(t) = 2r\Omega \qquad (35b)$$

$$K(t) = \Omega^2 \qquad (35c)$$

3. Results and discussions

A simply supported beam (Figure 3) with the following characteristics is considered where a non-ideal backlash support is located in the middle of the beam. Unless stated otherwise, all numerical results presented in this section are based on the following numerical data:

L=50 m, E=2.0×10^{11} N.m^{-2}, I=0.0417 m^4, m=3930 kg.m^{-1}, M=39300 kg, A=0.5 m^2, δ_{cr}=0.8 δ_{st}, v=100 m.s^{-1}, g=9.81 m.s^{-2}, L$_S$/L=0.5, height=1.0 m, width=0.5m, r$_1$=r$_2$=0.1.

in which δ_{st} is the static deflection due to the moving mass M at mid-span and is equal to $MgL^3/48EI$. In this study, a new mass is assumed to enter the beam domain from the left as soon as the old one exits it from the right, the process being repeated for an arbitrary number. For the next step, it is now required to consider the state variables at the end of each moving mass traveling as initial conditions.

Here, five methods are applied to analyze the dynamical system: the dynamic trajectories, power spectra, Poincaré maps, Lyapunov exponent and bifurcation diagrams. These properties are all used together to determine more accurately the onset conditions for the chaotic motion. The dynamic orbit can only be used to distinguish whether the system is periodic or non-periodic and it cannot provide enough information to predict the onset for the chaotic motion. Therefore, the usage of other analytical methods is necessary. The Poincaré section is a hyper-surface in the state space transverse to the flow of a given system. In non-autonomous systems, points on the Poincaré section represent the return points of the time series at a constant interval T, where T is the driving period of the exciting force that is here the time for one travelling of the moving mass along the beam. For chaotic motion, the return points in the Poincaré map form a particular pattern or many irregular points. For nT-periodic motion, the return points in the Poincaré map include n discrete points. A bifurcation diagram provides a summary of the essential dynamics of the system and is therefore a useful way for observing the system non-linear dynamic behaviour. There are many publications on nonlinear dynamic systems and methods used to analyze them. For the sake of brevity, we do not explain them in this paper and instead refer the interested readers to references [34-36]. To generate a bifurcation diagram, one control parameter is varied with a constant step and the state variables at the end of one integration step are used as the initial values for the next step.

The gap ratio, s, that is defined as the ratio between δ_{cr} and δ_{st} is used as the first control parameter. The value of it varies from zero, for an ideal support, to 1.2 in Figures 3 and 4. These figures are the bifurcation diagrams of the beam center with a non-ideal support where the gap ratio is considered as the control parameter. The bifurcation diagram for the case of moving mass formulation is considered in Figure 3 while Figure 4 indicates the bifurcation diagram for the case of moving forces instead of moving masses. For the moving force formulation, the terms due to the Coriolis, centrifugal, and inertia [Eq. (8a, 8b)] forces are neglected. The simulation results in Figure 3 show that the vibration amplitude of the beam center has its lowest value when the gap ratio is either zero, or very small. The dynamic responses for small gap ratio are synchronous with period-one. It proves that for zero or low values of the gap, i.e. the backlash is zero or negligible, the system often keeps regular vibration or periodic vibration because of the small nonlinearity. The amplitude becomes gradually larger as the gap

ratio increases. The largest amplitude for a periodic response occurs at $s = 1.06$ with a normalized amplitude of 1.22. An interesting result is also found for beam responses at $s = 0.129$, 0.286 and 1.22: the so-called "jump phenomenon". Also, over the range $s = 0.672 \sim 0.838$ the chaotic motion was observed.
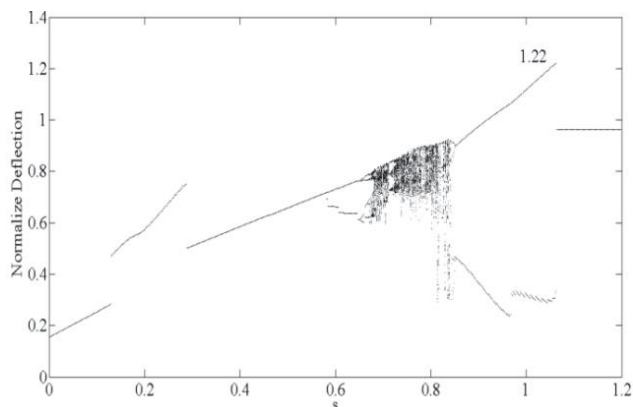

Figure 3: Bifurcation diagram of the beam center for the case of the moving mass formulation when the gap ratio is used as the control parameter
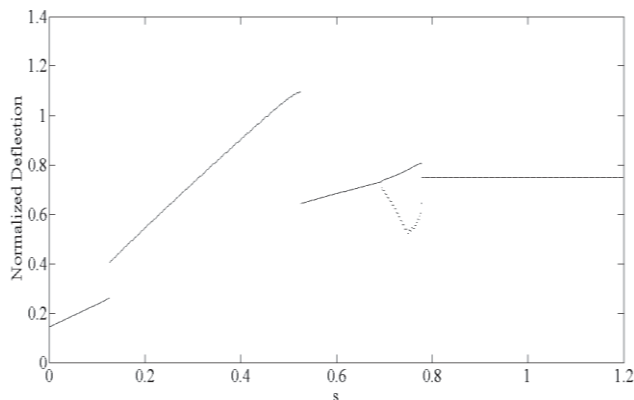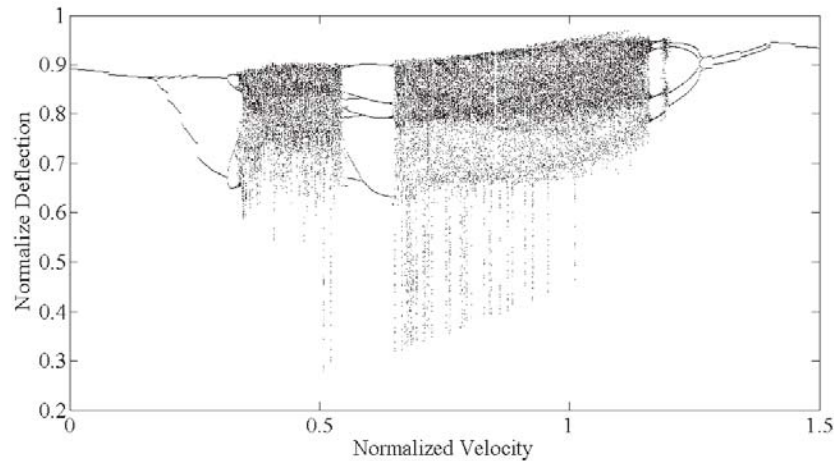

Figure 4: Bifurcation diagram of the beam center for the case of the moving force formulation when the gap ratio is used as the control parameter

Figure 4 shows a different scenario for the case of moving load formulation. In this figure, the nonlinear terms related to the moving mass formulation have been neglected. The chaotic motions have not been observed in the studied range of parameters. This difference between two diagrams (i.e. Figures 3, 4) is due to the effects of the moving mass which together with the nonlinear support terms lead to more severe nonlinear motion of the system as shown in Figure 3.

One may use the gap ratio, s as a control parameter by reversing it. If s decreases from a value to zero, a different bifurcation diagram may be obtained. Figure 5a,b shows the bifurcation

diagrams when s increases and then decreases for the case of moving mass and moving force, respectively. Closed loops due to nonlinear support are seen in this figure, created around the points where jump phenomena have occurred. These loops imply that more than one stable solution exists for some values of the gap ratio. In this figure, the dash lines indicate the jumping phenomena.

(a)

(b)
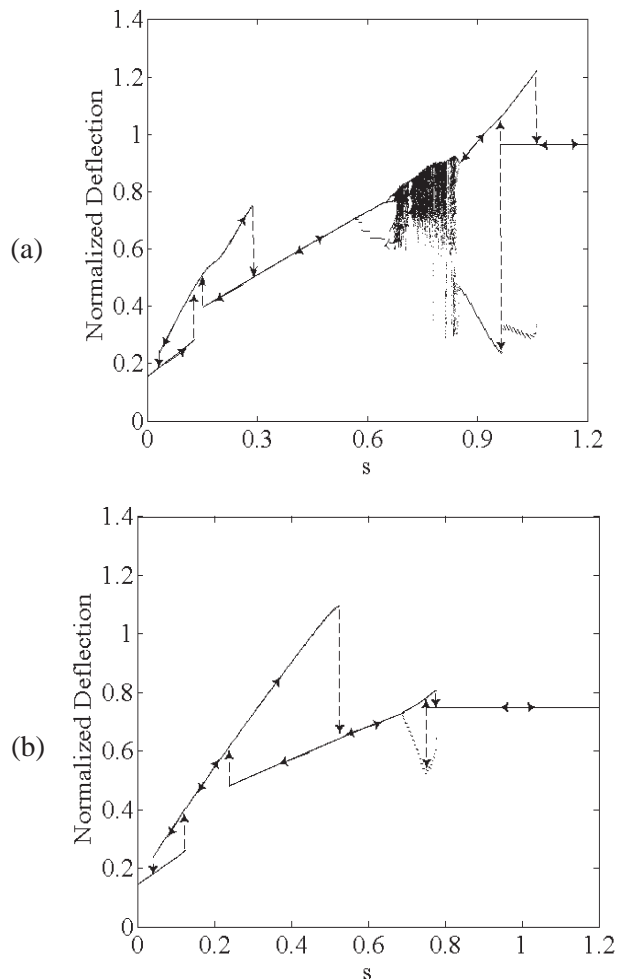
Figure 5: Bifurcation diagram of the beam center when the gap ratio as the control parameter, increases and then decreases: (a) Case of the moving mass; (b) Case of the moving force

Figure 6 is the bifurcation diagram of the beam center when the velocity is used as a control parameter. In this figure, x-axis represents the normalized velocity of the moving mass, $\tilde{V}$, which has been normalized with respect to the critical velocity for a simply supported Euler-Bernoulli beam that is defined as [6]

$$V_{cr} = \frac{\omega_1 L}{\pi} \tag{36}$$

where ω_1 is

$$\omega_1 = \sqrt{\frac{EI}{m}\left(\frac{\pi}{L}\right)^2}$$ (37)

In Figure 6, the chaotic motion is shown over the ranges $\tilde{V} = 0.338 \sim 0.543$, $0.650 \sim 1.165$ and $1.182 \sim 1.198$. A process of period doubling bifurcation is observed over the ranges $\tilde{V} = 0 \sim 0.337$, $0.544 \sim 0.649$, $1.166 \sim 1.181$ and $1.199 \sim 1.5$.

Figures 7–24 represent the time histories, phase diagrams, Poincaré´ maps, power spectrums and Lyapunov exponents of the beam center for the moving mass formulation at $s = 0.0$, 0.450, 0.640, 0.720, 0.770, 0.805, 0.850, 0.950 and 1.150, respectively. The results of the diagrams show that the dynamic response of the beam center is $1T$-periodic motion at $s = 0.0$, 0.450 and 1.150. At $s = 0.640$ and 0.950, the system becomes $2T$ and at $s = 0.850$, the system becomes $4T$-periodic motions, correspondingly. If at least one of the values of Lyapunov exponents is positive, the chaotic

phenomena will occur [36]. Considering three modes, six Lyapunov exponents are obtained. At values of $s = 0.720$, 0.770 and 0.805 (Figures 13–18) the dynamic trajectories are unstable and the number of excited frequencies becomes numerous. Periodic motion is no longer in existence at these values. Many discrete points in the Poincare´ maps and positive values of at least one of the Lyapunov exponents also indicate that the system motion is chaotic [34-36]. From these results, it can be seen that the moving mass-beam system undergoes a process of period doubling bifurcation as the gap ratio is increased over the range $s = 0.581 \sim 0.672$ and also undergoes a sudden transformation into chaos as the gap ratio is increased over the range $s = 0.672 \sim 0.838$. At higher values of the gap ratio, the dynamic behavior of the beam is found to be $4T$ - periodic at $s = 0.850$, $2T$ - periodic at $s = 0.95$ and $1T$-periodic for $s > 1.15$.

Figure 6: Bifurcation diagram of the beam center for the case of the moving mass formulation when the normalized moving mass velocity is used as the control parameter: $\tilde{V} = 0 \sim 1.5$
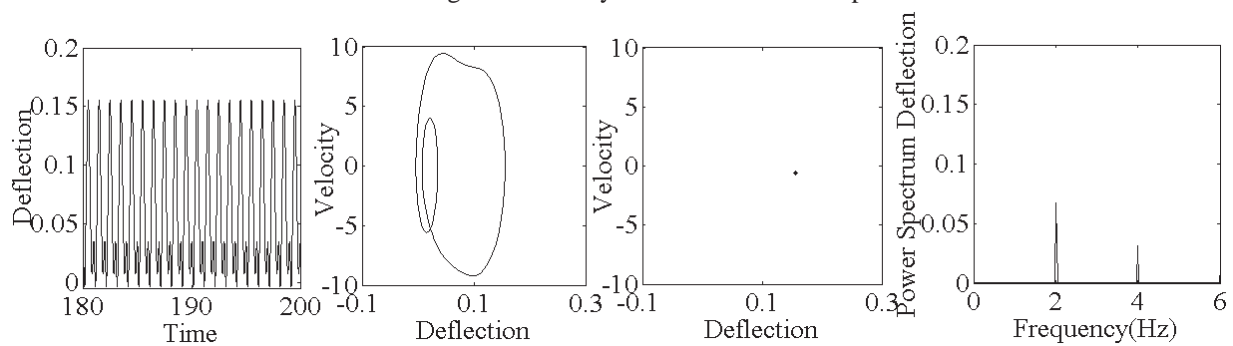

Figure 7: The time history, phase plane portrait, Poincaré map and power spectrum at $s = 0$
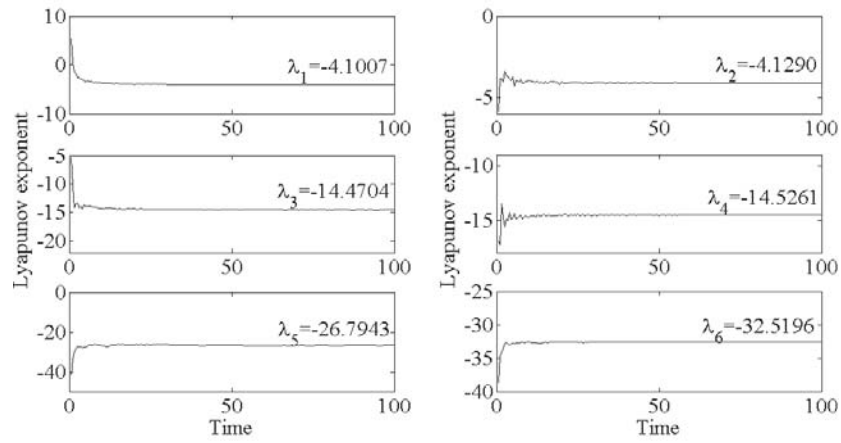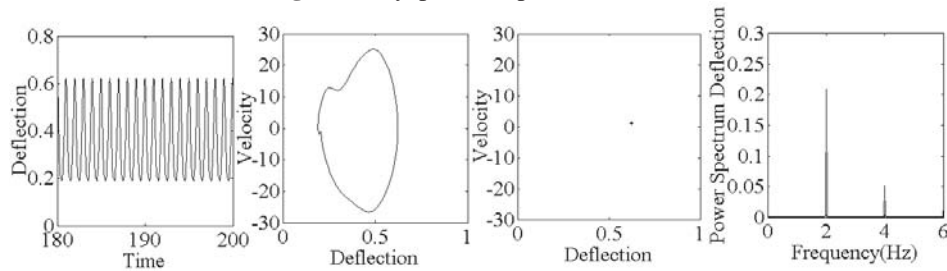
Figure 8: Lyapunov exponents at *s* = 0

Figure 9: The time history, phase plane portrait,
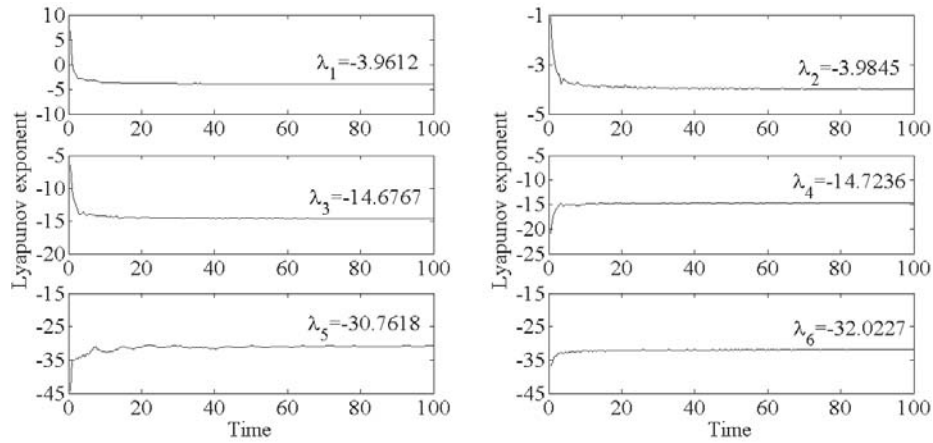Poincaré map and power spectrum at *s* = 0.450

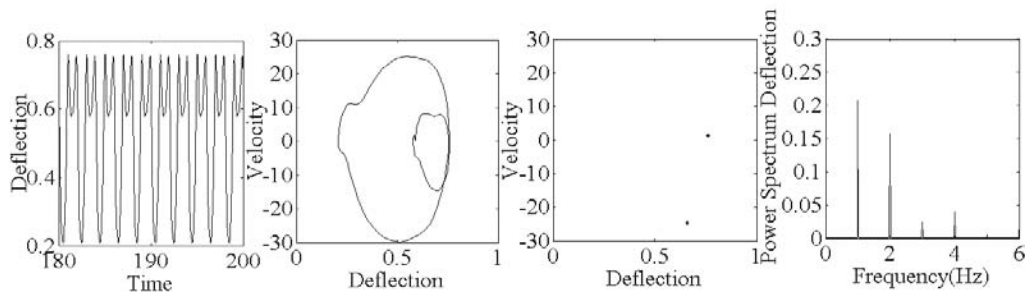**Figure 10:** Lyapunov exponents at *s* = 0.450

Figure 11: The time history, phase plane portrait,
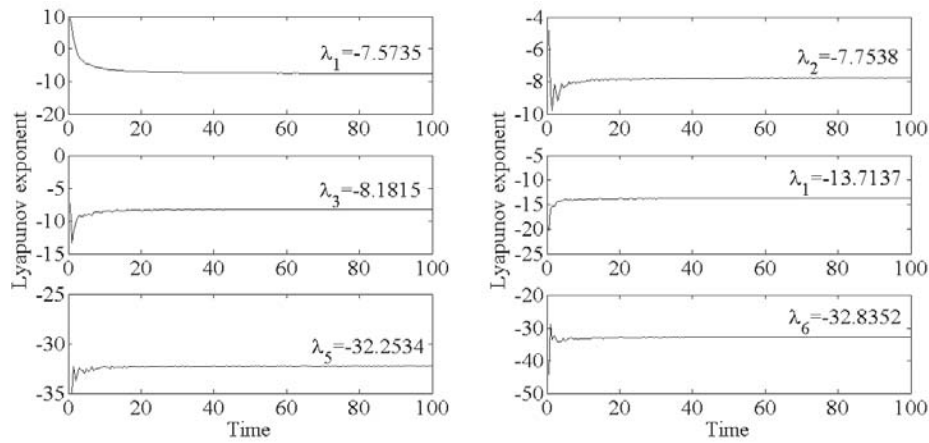Poincaré map and power spectrum at *s* = 0.640
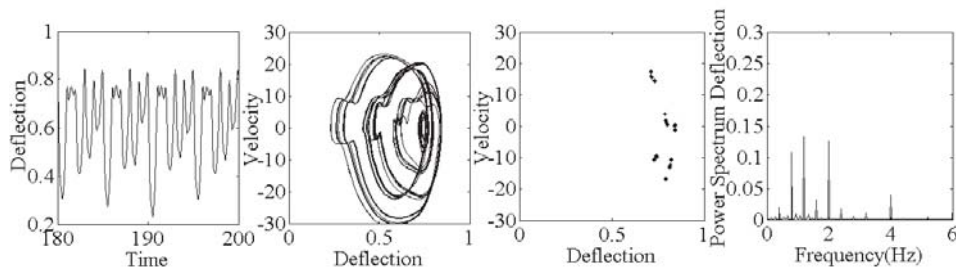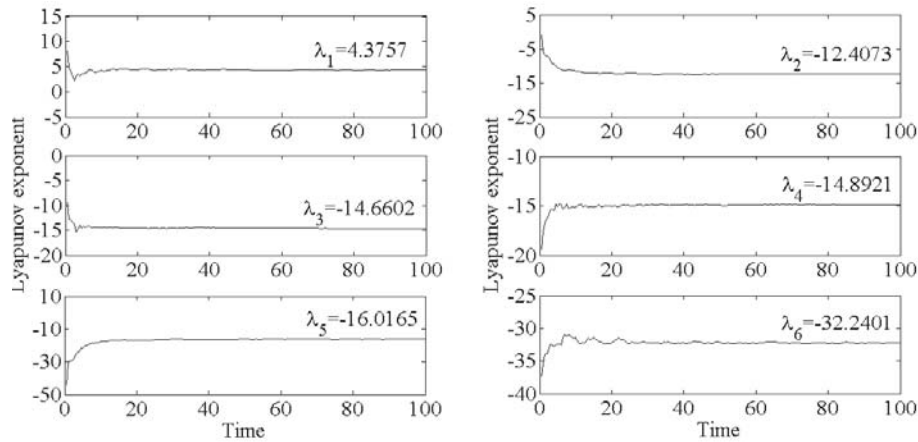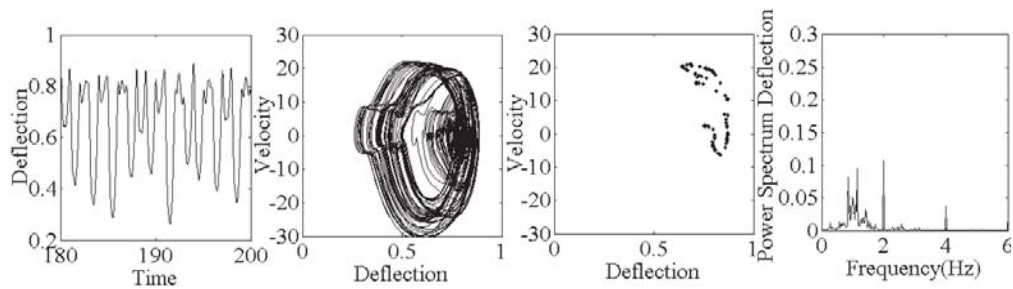
Figure 12: Lyapunov exponents at $s = 0.640$

Figure 13: The time history, phase plane portrait,
Poincaré map and power spectrum at $s = 0.720$

Figure 14: Lyapunov exponents at $s = 0.720$

Figure 15: The time history, phase plane portrait,
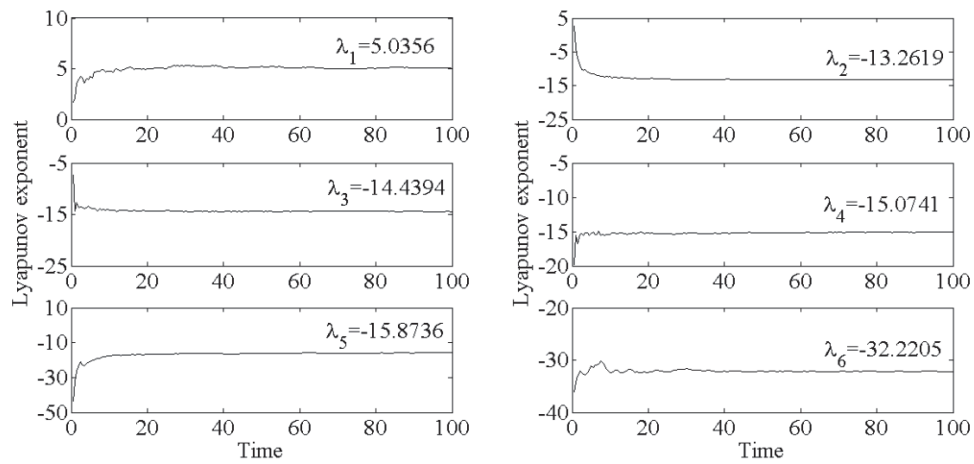Poincaré map and power spectrum at $s = 0.770$
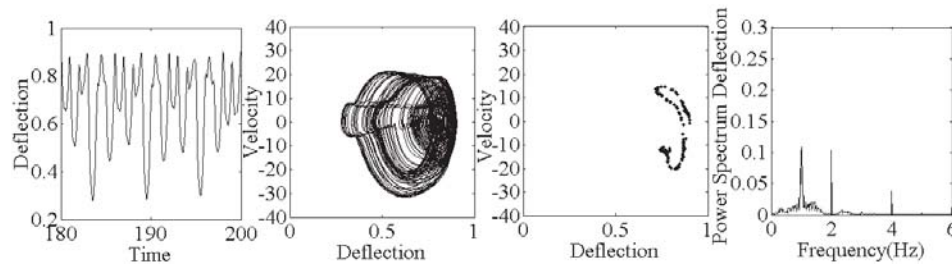
Figure 16: Lyapunov exponents at $s = 0.770$

Figure 17: The time history, phase plane portrait,
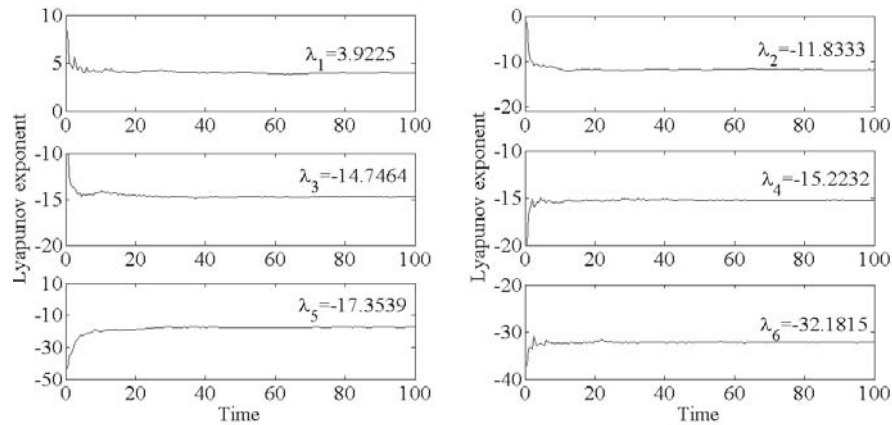Poincaré map and power spectrum at $s = 0.805$

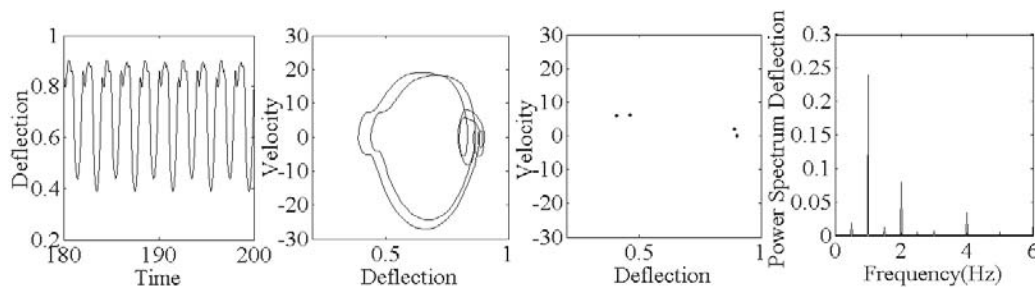**Figure 18:** Lyapunov exponents at $s = 0.805$

Figure 19: The time history, phase plane portrait,
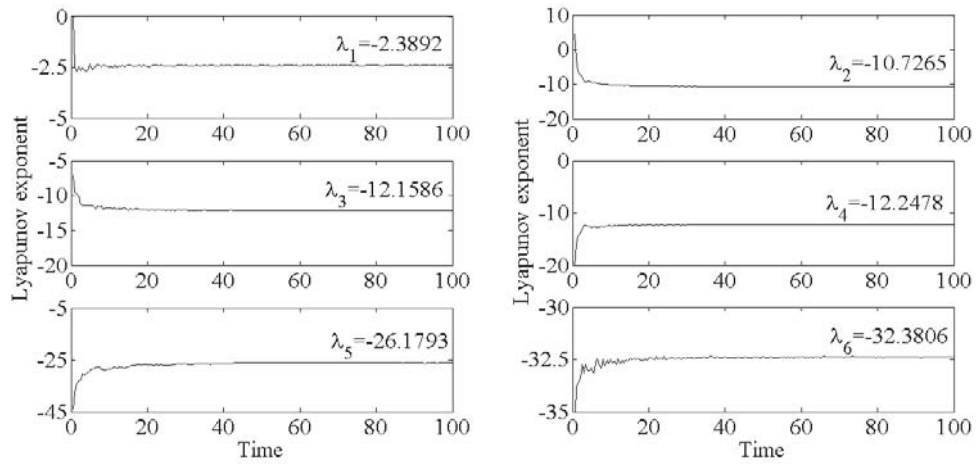Poincaré map and power spectrum at $s = 0.850$

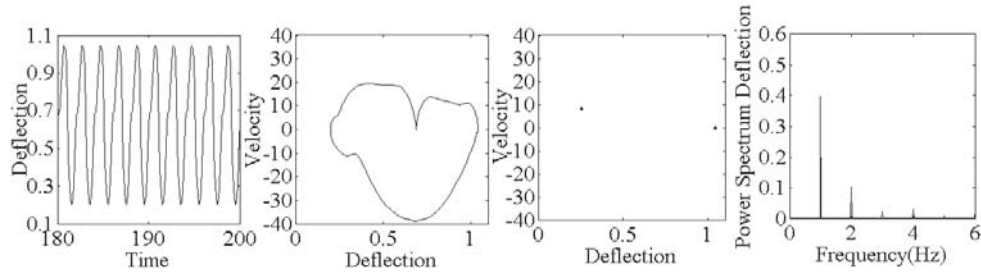**Figure 20:** Lyapunov exponents at $s = 0.850$

Figure 21: The time history, phase plane portrait, Poincaré map and power spectrum at $s = 0.950$
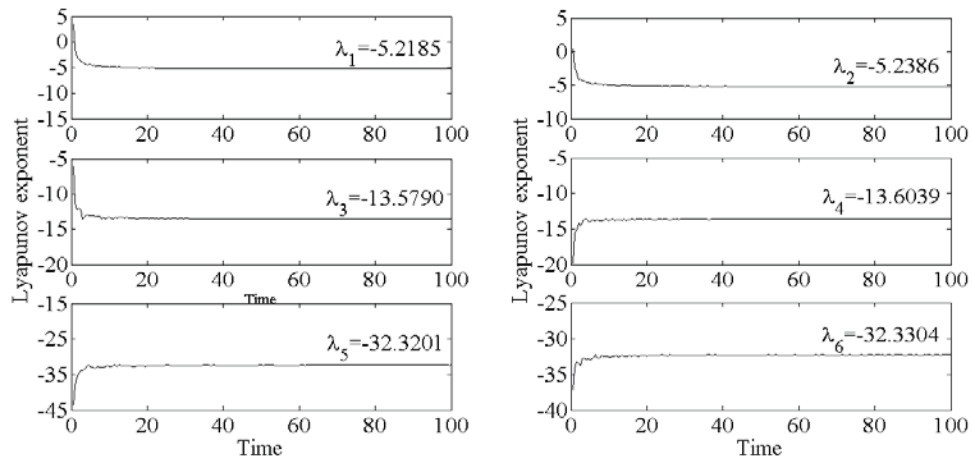
Figure 22: Lyapunov exponents at $s = 0.950$

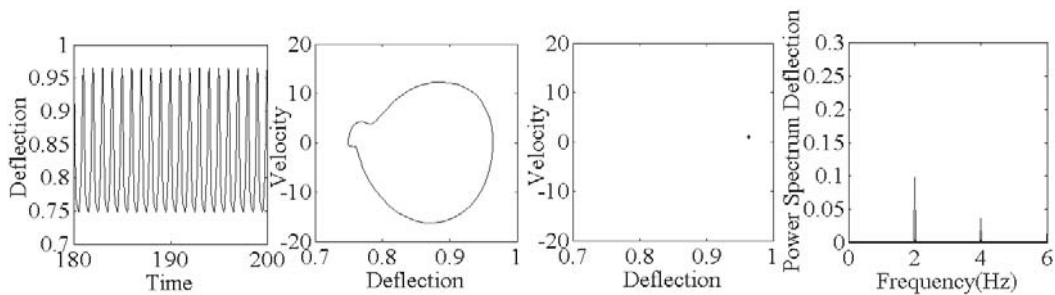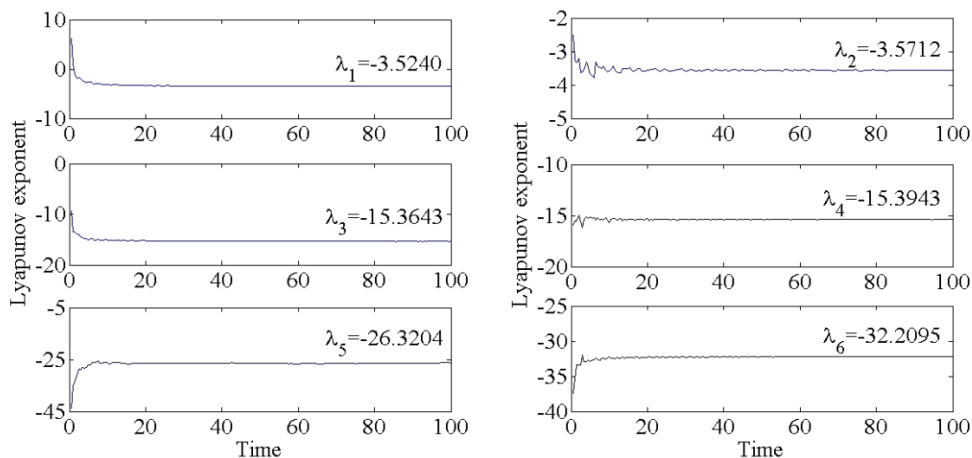**Figure 23:** The time history, phase plane portrait, Poincaré map and power spectrum at $s = 1.150$

Figure 24: Lyapunov exponents at $s = 1.150$

Table 1: Lyapunov exponents and state of the system

s	λ_1	λ_2	λ_3	λ_4	λ_5	λ_6	State
0	-4.1007	-4.1290	-14.4704	-14.5261	-26.7943	-32.5196	Period-1
0.450	-3.9612	-3.9845	-14.6767	-15.7236	-30.7618	-32.0227	Period-1
0.640	-7.5735	-7.7538	-8.5453	-14.0066	-32.2534	-32.8352	Period-2
0.720	4.3757	-12.4073	-14.6602	-14.8921	-16.0165	-32.2401	Chaos
0.770	5.0356	-13.2619	-14.4394	-15.0741	-15.8736	-32.2205	Chaos
0.805	3.9225	-11.8333	-14.7464	-15.2232	-17.3539	-32.1815	Chaos
0.850	-2.3892	-10.7265	-12.1586	-12.2478	-26.1793	-32.3806	Period-4
0.950	-5.0740	-5.2386	-13.5790	-13.6093	-32.3201	-32.3304	Period-2
1.150	-3.5340	-3.5712	-15.3643	-15.3943	-26.3204	-32.2095	Period-1

Table 1 shows the values of the Lyapunov exponents and the state of the system. According to Table 1, chaos phenomena does not occur for $s= 0$, 0.450, 0.640, 0.850, 0.950 and 1.150, however, for the values of $s = 0.720$, 0.770 and 0.805, chaos can be observed.

4. Conclusions

A simply supported Timoshenko beam with an intermediate non-ideal support subjected to a moving mass was considered. The analysis was employed in this study by calculating the dynamic trajectories of the beam center, power spectra, Poincaré maps, bifurcation diagrams and Lyapunov exponents. The dimensionless gap coefficient and the moving mass speed are used as control parameters. The numerical results reveal that the system exhibits a diverse range of periodic, sub-harmonic, and chaotic behaviors. The onset of chaotic motion is identified from the phase diagrams, power spectra, Poincaré maps and Lyapunov exponents of the system.

Furthermore, it is concluded that in this case when the terms due to the moving mass were neglected, the chaotic motion was not observed in the bifurcation diagram. It is also seen that if the gap ratio, s, increases and then decreases, two different bifurcation diagrams may be predicted. Created closed loops imply that more than one stable solution exists for some values of the gap ratio.

5. References

[1] S.G.G. Stokes, Discussion of a differential equation relating to the breaking of railway bridges, 1849.

[2] Commissioners appointed to inquire into the application of iron to railway structures, Report of the commissioners appointed to inquire into the application of iron to railway structures, William Clowes, Great Britain (1849).

[3] Y. Chen, Distribution of vehicular loads on bridge girders by the FEA using ADINA: modeling, simulation, and comparison, Computers & structures, 72 (1999) 127-139.

[4] T. Wu, D. Thompson, The effects of local preload on the foundation stiffness and vertical vibration of railway track, Journal of Sound and Vibration, 219 (1999) 881-904.

[5] M. Todd, S. Vohra, Shear deformation correction to transverse shape reconstruction from distributed strain measurements, Journal of sound and vibration, 225 (1999) 581-594.

[6] L. Fryba, Vibration of solids and structures under moving loads, Thomas Telford, 1999.

[7] J.E. Akin, M. Mofid, Numerical solution for response of beams with moving mass, Journal of Structural Engineering, 115 (1989) 120-131.

[8] M. Mofid, J.E. Akin, Discrete element response of beams with traveling mass, Advances in Engineering Software, 25 (1996) 321-331.

[9] D. Younesian, M. Kargarnovin, D. Thompson, C. Jones, Parametrically excited vibration of a timoshenko beam on random viscoelastic foundation jected to a harmonic moving load, Nonlinear Dynamics, 45 (2006) 75-93.

[10] A. Yavari, M. Nouri, M. Mofid, Discrete element analysis of dynamic response of Timoshenko beams under moving mass, Advances in engineering software, 33 (2002) 143-153.

[11] S. Ziaei-Rad, A. Ariaei, M. Imregun, Vibration analysis of Timoshenko beams under uniform partially distributed moving masses, Proceedings of the Institution of Mechanical Engineers, Part K: Journal of Multi-body Dynamics, 221 (2007) 551-566.

[12] H. Merta, Characteristic time series and operation region of the system of two tank reactors (CSTR) with variable division of recirculation stream, Chaos, Solitons & Fractals, 27 (2006) 279-285.

[13] T. Stachowiak, T. Okada, A numerical analysis of chaos in the double pendulum, Chaos, Solitons & Fractals, 29 (2006) 417-422.

[14] S. Gakkhar, B. Singh, Complex dynamic behavior in a food web consisting of two preys and a predator, Chaos, Solitons & Fractals, 24 (2005) 789-801.

[15] J. Dejonckheere, S.M. Disney, M.R. Lambrecht, D.R. Towill, The impact of information enrichment on the bullwhip effect in supply chains: A control engineering perspective, European Journal of Operational Research, 153 (2004) 727-750.

[16] S. Gakkhar, B. Singh, Dynamics of modified Leslie–Gower-type prey–predator model with seasonally varying parameters, Chaos, Solitons & Fractals, 27 (2006) 1239-1255.

[17] J.-G. Zhang, J.-N. Yu, Y.-D. Chu, X.-F. Li, Y.-X. Chang, Bifurcation and chaos of a non-autonomous rotational machine systems, Simulation Modelling Practice and Theory, 16 (2008) 1588-1605.

[18] Z.-M. Ge, J.-K. Lee, Chaos synchronization and parameter identification for gyroscope system, Applied mathematics and computation, 163 (2005) 667-682.

[19] G. M Mahmoud, A. A Mohamed, S. A Aly, Strange attractors and chaos control in periodically forced complex Duffing's oscillators, Physica A: Statistical Mechanics and its Applications, 292 (2001) 193-206.

[20] L.-Q. Chen, Y.-Z. Liu, A modified exact linearization control for chaotic oscillators, Nonlinear Dynamics, 20 (1999) 309-317.

[21] Z.-M. Ge, W.-Y. Leu, Anti-control of chaos of two-degrees-of-freedom loudspeaker system and chaos synchronization of different order systems, Chaos, Solitons & Fractals, 20 (2004) 503-521.

[22] H.-K. Chen, Z.-M. Ge, Bifurcations and chaos of a two-degree-of-freedom dissipative gyroscope, Chaos, Solitons & Fractals, 24 (2005) 125-136.

[23] Z.-M. Ge, Y.-S. Chen, Adaptive synchronization of unidirectional and mutual coupled chaotic systems, Chaos, Solitons & Fractals, 26 (2005) 881-888.

[24] M. Pakdemirli, H. Boyaci, Effect of non-ideal boundary conditions on the vibrations of continuous systems, Journal of Sound and Vibration, 249 (2002) 815-823.

[25] M. Pakdemirli, H. Boyaci, Vibrations of a stretched beam with non-ideal boundary conditions, Math. Comput. Appl, 6 (2001) 217-220.

[26] M. Pakdemirli, H. Boyacı, Non-linear vibrations of a simple–simple beam with a non-ideal support in between, Journal of sound and Vibration, 268 (2003) 331-341.

[27] R. Lin, D. Ewins, Chaotic vibration of mechanical systems with backlash, Mechanical Systems and Signal Processing, 7 (1993) 257-272.

[28] H.-P. Lin, Direct and inverse methods on free vibration analysis of simply supported beams with a crack, Engineering structures, 26 (2004) 427-436.

[29] I.H. Shames, Energy and finite element methods in structural mechanics, CRC Press, 1985.

[30] C. Bilello, L. Bergman, Vibration of damaged beams under a moving mass: theory and experimental validation, Journal of Sound and Vibration, 274 (2004) 567-582.

[31] H.-P. Lin, S.-C. Chang, Forced responses of cracked cantilever beams subjected to a concentrated moving load, International journal of mechanical sciences, 48 (2006) 1456-1463.

[32] M. Dadfarnia, N. Jalili, E. Esmailzadeh, A comparative study of the Galerkin approximation utilized in the Timoshenko beam theory, Journal of sound and vibration, 280 (2005) 1132-1142.

[33] M. Mahmoud, M. Abou Zaid, Dynamic response of a beam with a crack subject to a moving mass, Journal of Sound and Vibration, 256 (2002) 591-603.

[34] A.H. Nayfeh, B. Balachandran, Applied nonlinear dynamics: analytical, computational and experimental methods, John Wiley & Sons, 2008.

[35] A. Nayfeh, D. Mook, Nonlinear oscillations, 1979, John Willey and Sons, New York.

[36] F.C. Moon, Chaotic vibrations: an introduction for applied scientists and engineers, Research supported by NSF, USAF, US Navy, US Army, and IBM. New York, Wiley-Interscience, 1987, 322 p., 1 (1987).